ABSORPTION OF CO2 LASER LIGHT BY A DENSE, HIGH TEMPERATURE PLASMA

N. Peacock, M. Forrest, P. Morgan, M. Goldman, T. Rudolph, A. Offenberger

ABSORPTION OF CO_2 LASER LIGHT BY A DENSE, HIGH TEMPERATURE PLASMA

N. J. PEACOCK, M. J. FORREST, P. D. MORGAN (*),
M. V. GOLDMAN (**), T. RUDOLPH (**), A. A. OFFENBERGER (***)

Culham Laboratory, Abingdon, Oxon. OX14 3DB, U. K.
(Euratom/UKAEA Fusion Association)

Résumé. — L'interaction entre le faisceau pulsé d'un laser au CO_2 et le plasma produit par un dispositif *plasma focus* est examinée des points de vue théorique et expérimental. Le faisceau du laser CO_2, qui est dirigé perpendiculairement à l'axe, suivant le gradient de densité, ne perturbe que faiblement le plasma car la densité de rayonnement de 30 J cm^{-3} (compte tenu du facteur d'amplification de Airy) est néanmoins plus faible que l'énergie thermique du plasma ($\lesssim$ 1 kJ cm^{-3}). Au contraire, le rayon du laser est fortement affecté par le plasma.

Durant la phase de compression en *pinch* quand la fréquence du plasma $\omega_{pe} > \omega_{CO_2}$, l'absorption du faisceau est beaucoup plus importante que celle prévue en utilisant la résistivité classique.

Les fluctuations de densité à la fréquence de Langmuir sont mesurées directement par diffusion frontale à l'aide du faisceau sonde d'un laser à rubis. Etant donné que les nombres d'ondes correspondent à $(K\lambda_D) \sim 0{,}1$ les ondes de Langmuir devraient apparaître dans le sepctre diffusé comme des raies électroniques, décalées de 427 Å par rapport à la longueur d'onde du laser à rubis. A faible intensité de pompage du laser au CO_2, l'intensité des ondes électroniques est proche du niveau thermique. Si on augmente l'intensité de pompage au-delà d'un seuil de 3×10^9 W/cm^{-2}, on observe une forte augmentation du rayonnement diffusé, qui peut dépasser d'un facteur 30 le niveau thermique.

L'étude WKB de l'instabilitité de dégénérescence électron-ion est en assez bon accord avec les mesures. Cette étude tient compte de la croissance linéaire des ondes à température électronique et ionique égales, et des phonomènes de convection dans un plasma inhomogène.

Abstract. — The interaction between a pulsed, CO_2 laser beam and the plasma produced in a plasma focus device is investigated theoretically and experimentally. The CO_2 laser radiation, directed orthogonal to the pinch axis and along the density gradient only weakly perturbs the focus since the radiation density of 30 J cm^{-3} (allowing for the Airy enhancement factor near the critical layer), is still less than the plasma thermal energy $\gtrsim$ 1 kJ cm^{-3}. On the contrary, the CO_2 laser beam is grossly affected by the plasma and absorption during the compressed pinch phase when the plasma frequency $\omega_{pe} \gtrsim \omega_{CO_2}$ is much more complete than can be predicted by classical resistivity.

Density fluctuations at the Langmuir frequency are measured directly by forward scattering from a probe, ruby laser beam. Since the wave numbers correspond to $(K\lambda_D) \sim 0.1$ the Langmuir waves should appear as electron ' lines ' in the scattered spectrum shifted by 427 Å from the ruby laser wavelength. At low CO_2 laser pump intensity the electron wave intensity is close to the thermal level. As the pump is increased beyond a threshold of $\sim 3 \times 10^9$ W/cm^{-2} (in vacuo) enhanced scattering is observed, reaching a factor of 30 above thermal.

A WKB treatment of the electron-ion decay instability which takes into account the linear growth of waves at equal electron and ion temperatures and their convection in an inhomogeneous plasma is reasonably consistent with the observations.

1. **Introduction.** — The aim of this paper is to report on the absorption and redistribution of energy in a CO_2 laser beam by a pre-formed and pre-heated plasma, in circumstances where anomalous heating processes might be expected. The plasma is the dense pinch formed in a plasma focus device [1].

In contrast to the many experimental studies which have been reported in the literature on laser beam interactions with solid [2, 3] or gaseous [4] targets, the use of a preformed plasma which is not substantially altered by the pump beam has a number of advantages. In the plasma focus the kinetic energy density is considerably higher than the threshold, radiation intensity required for the most readily-excited instabilities. Among these, there are, for example, the parametric decay instability [5, 6, 7], the oscillating two-stream instability [8] and the

(*) Now at Ecole Polytechnique Fédérale de Lausanne, Switzerland.

(**) University of Colorado, Boulder, U. S. A.

(***) University of Alberta, Edmonton, Canada.

stimulated Brillouin instability, all of which can be excited with pump intensities between 10^{10} and 10^{12} W/cm^{-2}.

During the pinch compression phase of the plasma focus the electron plasma frequency is matched to the frequency of infra-red light at least over a limited spatial region and for a limited time duration. A CO_2 laser operating at 10 microns wavelength might be expected to act therefore as a pump for Langmuir waves in the plasma.

The focus device has been relatively well diagnosed by a number of groups [9, 10, 11], and using a variety of measurement techniques ; but this advantage is to be offset against its somewhat irreproducible characteristics and inherent density fluctuations which, for certain wave-vectors, can be considerably above the thermal level due to current-driven instabilities [12].

In this study we observe absorption of the pump beam and enhancement of the Langmuir wave intensity when a CO_2 laser irradiates the partially-compressed pinch. The enhancement is described in terms of non-linear processes induced by the pump beam.

2. **Plasma characteristics with no external pump beam.** — The evolution of the highly-compressed plasma in a Mather type, open-ended, coaxial gun focus is shown schematically in figure 1. The dimensions of the inner and outer electrodes are 5 cm and 10 cm respectively. The stored energy in the capacitor bank is 40 kJ at 30 kV and the ambient filling pressure of deuterium is between 2.5 and 3.0 torr.

Time-resolved interferograms of the converging, cusped, conical plasma front are shown in figure 2 and the density distributions, suitably Abel-inverted, are shown as a function of time in figure 3. It is to be noted that the density has a peak value of the order of 3×10^{19} cm^{-3} and it remains higher than

$$n_{ec} = 9.94 \times 10^{18} \text{ cm}^{-3},$$

the critical density, for reflection of the CO_2 laser light, for several tens of nanoseconds. During the late stage of the compression of the plasma onto the axis of symmetry of the coaxial electrodes, the scale length for the density gradient,

$$L = \left[\frac{1}{n_e}\frac{\partial n_e}{\partial r}\right]^{-1},$$

changes rapidly in time, figure 4. Typically L will vary from 0.3 to 0.03 cm in the 40 nanoseconds up to peak compression.

The particle energy distribution and the background level of turbulence in the plasma has been measured in some detail [11, 13] using the scattered light from ruby laser probes. Most of the analyses have been based on the intensity and frequency spread of the *ion feature* in the scattered light spectrum. Samples [13] of the spectral broadening, $\Delta\omega = 1.6\ Kv_i$, where v_i is the ion thermal velocity and K the differential scattering wavenumber, are shown for values of the scattering parameter, $(K\lambda_D)^{-1}$, between 1 and 2, in figure 5. The experimental points have been fitted to thermal distributions of the electrons and ions following Evans (1970) [14].

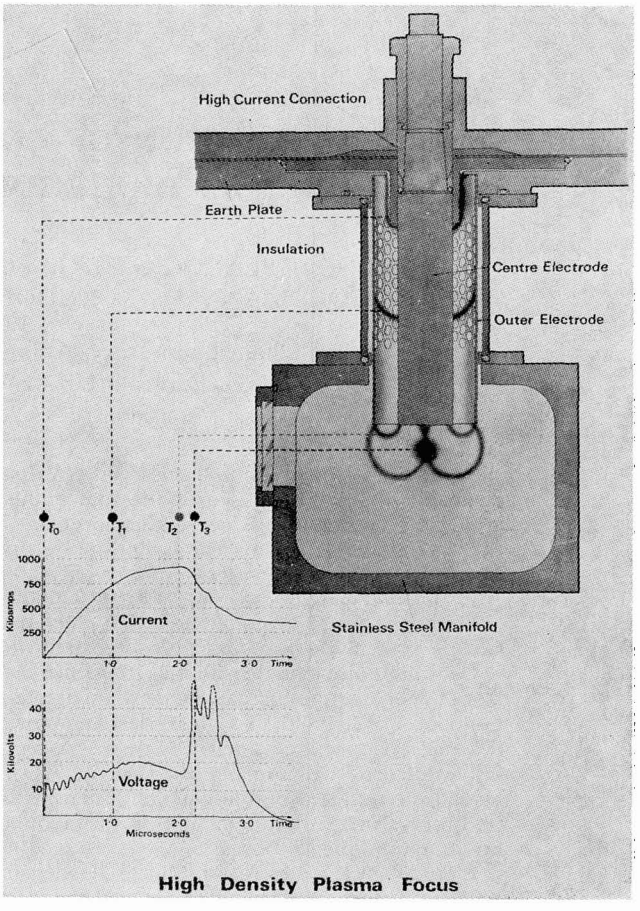

FIG. 1. — Schematic diagram of the spatial variation in the location of the plasma boundary and the associated electric waveforms in the plasma focus device.

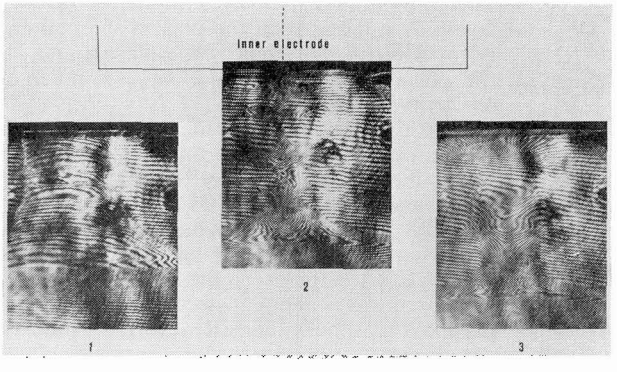

FIG. 2. — One nanosecond exposure time sequence of three interferograms at — 30, 0 and + 30 nanoseconds where time *0* refers to moment when the compression front first reaches the axis of symmetry on Plasma Focus.

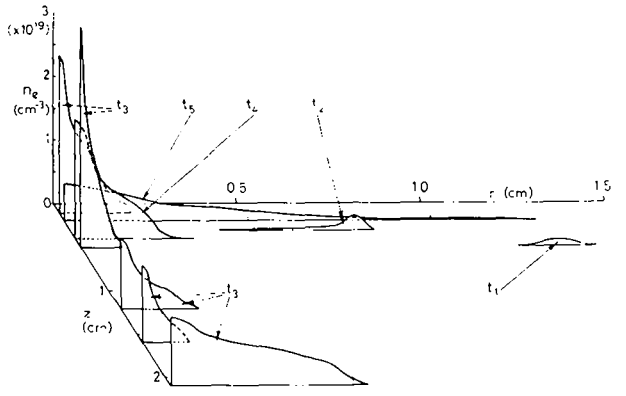

FIG. 3. — Temporal variation of density distribution in the plasma focus, after Abel inversion t_1, $t_2 \ldots t_5$ denotes a time sequence lasting 150 ns, with t_3 corresponding to peak compression.

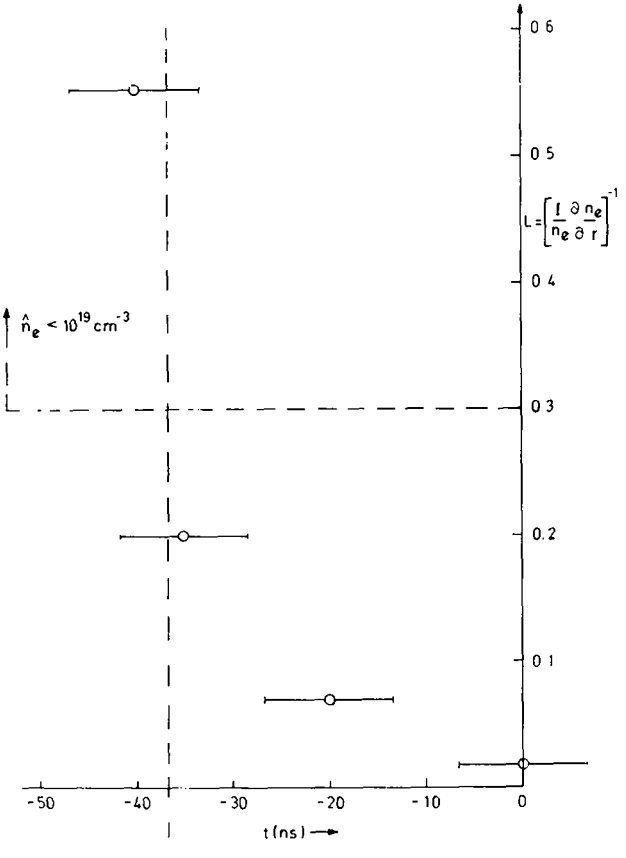

FIG. 4. — Temporal variation of the radial density scale length,

$$L\,(\mathrm{cm}) = \left[\frac{1}{n_e}\frac{\partial n_e}{\partial r}\right]^{-1},$$

in the plasma focus, derived from interferometry. For

$$n_e < 10^{19}\ \mathrm{cm}^{-3}$$

the scale length is measured at the peak of the density profile while for $n_e > 10^{19}$, the scale length is appropriate to the pump beam, cut-off density, $n_{ec} = 9.94 \times 10^{18}\ \mathrm{cm}^{-3}$.

The maximum ion and electron temperatures occur at peak compression and are of the same order, i. e. $\hat{T}_e \simeq \hat{T}_i \simeq 2$ keV. An adiabatic scaling, $T_e\, r^{2(\gamma-1)} =$ constant, is appropriate to the fluid model constructed by Potter (1971) [15], and has

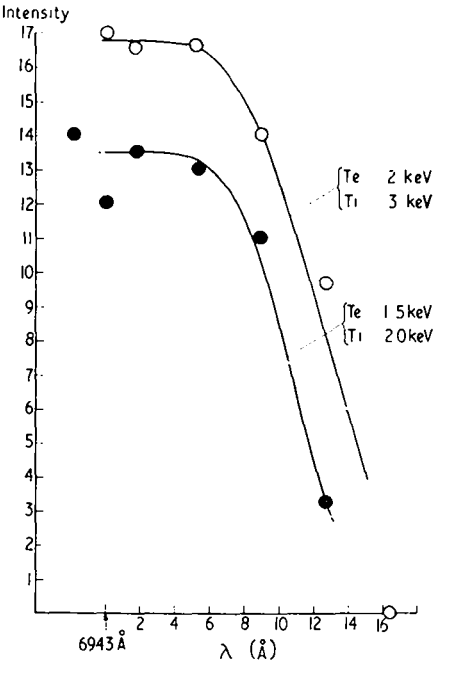

FIG. 5. — Electron and ion temperatures at peak compression derived from the collective, $K\lambda_D = 0.56$, ion feature of the scattered visible light spectrum. Forrest and Peacock (1974).

been used to calculate the variation in the peak temperature during the compression, figure 6.

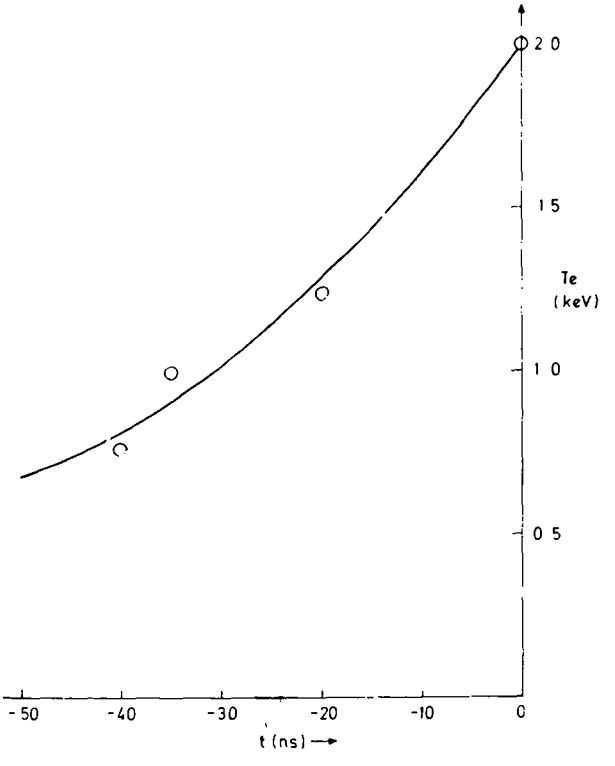

FIG. 6. — Variation in peak temperature during the pinch phase of the plasma focus, assuming 2-dimensional adiabatic compression.

The scattered light intensity in the ion feature is measured on an absolute basis and is given by

$$I_s = I_0 \cdot V_s \cdot \frac{d\Omega_s}{2\pi} \cdot \sigma_T \cdot n_e \int_0^{2k v_i} S(\omega, k)\, d\omega \qquad (1)$$

where I_0 is input ruby laser intensity and V_s and $d\Omega_s$ are the scattering volume and solid angle respectively, subtented by the detector. σ_T is the Thomson scattering cross-section. For $\alpha = (K\lambda_D)^{-1} \sim 1$, the factor

$$[n_e\, S(K)] = \frac{n_e}{(1 + \alpha^2)},$$

for a thermal plasma. In these experiments [13] we find $[n_e\, S(K)] \simeq 2\, n_e$, indicating a nearly thermal plasma for scattering vectors, $\bar{K}_\perp$ orthogonal to the current flow, $\bar{j}$. In complementary studies [11], Bernard and co-authors have found a somewhat similar level of background wave activity with, again, $[n_e\, S(K)] \simeq n_e$ for $\bar{K}_\perp \cdot \bar{K}_\parallel$. However for scattering vectors, $\bar{K}_\parallel$, parallel to $\bar{j}$, there is considerable enhancement above the thermal level, as shown in figure 7, especially at around 3 torr ambient pressure, which is our present operating conditions.

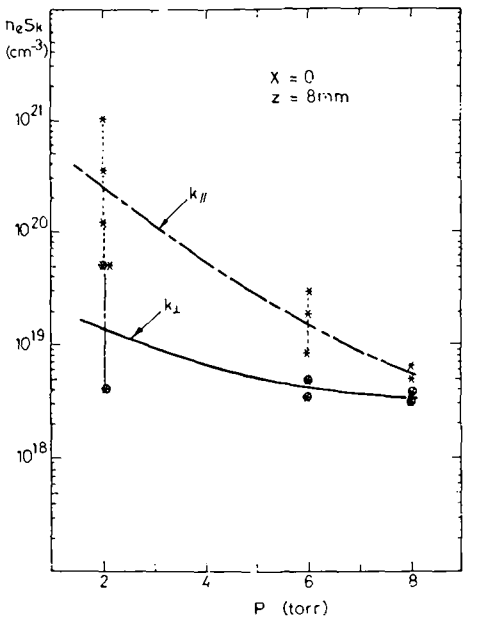

FIG. 7. — Absolute level of the collective ion feature, $K_D/K_\perp$ and $K_D/K_\parallel \gg 1$, in the spectrum of scattered ruby laser light from the plasma focus. The level is expressed in terms of the product of electron density and the dynamic form factor for the scattered light spectrum, $S(K)$. p (torr) is the ambient filling density, x and z are the radial and axial positions, in cylindrical coordinates, of the plasma responsible for scattering the laser light. $\bar{K}_\parallel$ and $\bar{K}_\perp$ refer to differential scattering vectors parallel and orthogonal respectively to the current flow; Bernard *et al.* (1974).

3. **Irradiation of the Focus Plasma by a CO_2 Laser Beam.** — A double discharge TEA, CO_2 laser delivering 10 joules in an initial, gain switched pulse of 40 ns duration has been used to irradiate plasma orthogonal to the pinch axis of symmetry. The experimental arrangement is shown in figure 8. After

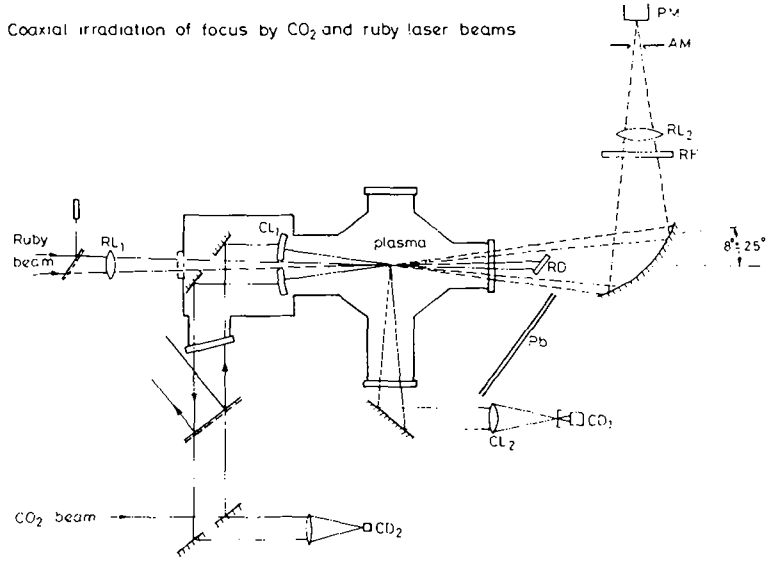

FIG. 8. — Optical layout (Plan-view) of the CO_2 laser interaction experiment with the dense plasma focus. The ruby laser probe beam and associated visible light scattering optics are coaxial with the CO_2 beam. Input of CO_2 laser beam, 10 → 20 J/50 ns, enters focus chamber (from below) via KCl beam splitter and Ge window. It is then focused via a F/5.5 germanium lens (CL_1) onto the plasma axis. Refracted CO_2 laser light is detected at 45°, 90° and 135° to incident beam and focused via a KCl lens (CL_2) onto appropriate detectors; CD_1 is a sensitive Au-doped Ge or Pb : Sn : Te photodetector shielded from the discharge with lead (Pb). CD_2 is a photon drag detector. Input of the ruby laser beam, 5 J/18 ns, enters chamber from left and is focused onto the axis of the plasma via a glass lens (RL_1). The ruby light dump (RD) completely attenuates the primary probe beam but scattered ruby laser light is detected (PM) through a narrow band filter, 6.500 ± 25 Å (RF), lens (RL_2) and azimuthal mask (AM).

losses in the optics the average CO_2 laser intensity, focussed in vacuo through an F/5.5 germanium lens on a 0.75 mm spot at the focus axis, is

$$2 \times 10^{10} \text{ W/cm}^{-2} .$$

Mode beating during the irradiation pulse will result in peak values of twice this intensity. Polarisers made from KCl plates inside the oscillator cavity ensure that 95 % of the output CO_2 laser energy is plane polarised [16]. The CO_2 laser beam is arranged to pump electron waves orthogonal to the density gradient with either p-type polarisation in which the electric vector, **E**, is orthogonal to $\bar{j}$, or alternatively s-type polarisation with **E** parallel to $\bar{j}$. The incident intensity, transmission, refraction and back-scatter of the CO_2 beam are measured by photon drag detectors, or Au-doped Ge, and Pb ; Sn ; Te detectors, the last two being liquid N_2-cooled, ensuring a wide range of detectivities for the infra-red radiation. A summary of the parameters of the irradiation conditions is shown in table I.

The effect of the plasma on the pump beam is taken into account in table I. In particular, the intensity, swollen by the Airy peaks near the critical surface, is given by

$$\Phi_{pl} \simeq \Phi_0 \text{ (vacuum)}/\eta_{min} , \qquad (2)$$

where η_{min} is the minimum value of the refractive index compatible with geometric optics,

$$\eta_{min}^{-1} = 3.8(L\omega_0/c)^{1/3} .$$

This swelling factor allows the pump intensity to exceed the threshold for the instabilities listed in the table. The energy density in the beam is seen to be small compared to the plasma kinetic energy.

Before discussing the results of the CO_2 laser beam/plasma interaction it is instructive to consider theoretically the absorption and refraction in an inhomogeneous plasma in which classical resistivity is the only absorption mechanism. For a plane wave incident on a cylindrical plasma the reflectivity [17] is given by

$$R = \exp(-2p\cos^5\theta) \qquad (3)$$

where θ is the angle of the incident light to the radius normal and

$$p = \frac{16}{15} K_\nu L ,$$

where L is the density scale length and K_ν, the resistive absorption coefficient,

$$K_\nu = \omega_{pe}^2/c\omega_{CO_2}\,\tau(\omega_{CO_2}^2 - \omega_{pe}^2)^{1/2} \qquad (4)$$

where τ is the electron-ion collision time [18]. In our plasma conditions, the paraxial rays, only, will penetrate to the critical reflection surface and will therefore suffer the greatest absorption with

$$R_{parax} = \exp\left(-2\int_0^{L \text{ at turning point}} K(\nu)\,dl\right).$$

$$\sim 0.64 \text{ for } \begin{cases} L = 0.20 \text{ cm} \\ \hat{T}_e = 900 \text{ eV} \\ \hat{n}_e = 0.99\, n_{ec} . \end{cases}$$

Thus the back reflected light should be substantial when the plasma density exceeds the critical value for reflection i. e. when $n_{ec} \gtrsim 9.94 \times 10^{18} \text{ cm}^{-3}$. Other light rays will be refracted with little loss in light intensity as is illustrated for the plasma at peak compression in figure 9.

Following the logic that, on theoretical considerations only a relatively small fraction will be absorbed from the pump beam in the high temperature plasma, it is instructive to neglect absorption completely as in the model calculations shown in figure 10. In this figure the pump beam $I_0\, e^{-(r/r_0)^2}$ is incident from the right on a high temperature plasma, with a parabolic density distribution, whose peak density and radius correspond to those measured interferometrically during the pinch phase of the plasma. It is evident, figure 10, that in the under-dense plasma, the pump beam is transmitted without much deviation ; but that as the electron density reaches, or exceeds, n_{ec} then there is a rapid angular variation in the refracted light. For $n_e \gg n_{ec}$, the light is mainly refracted back towards the incoming beam.

TABLE I

Summary of parameters of CO_2 beam interaction with plasma focus

Focused pump-beam intensity	Cut-off density	Ratio of oscillatory to electron thermal velocities	Energy density in CO_2 beam	Plasma Parameters		
—	—	—	—	—	—	
Φ_0 (in vacuo)	n_{ec}	$V \sim /V_{th}$	$E^2/8\pi$ (in vacuo)	$\hat{n}_e$	$\hat{T}_e$	$L = \left(\frac{1}{n_e}\frac{\partial n_e}{\partial r}\right)^{-1}$
				cm^{-3}	eV	cm
$< 4 \times 10^{10} \text{ W/cm}^{-2}$	$9.94 \times 10^{18} \text{ cm}^{-3}$	~ 0.02	0.7 J/cm^{-3}	9.94×10^{18}	2,500	0.3 0.03
Φ_{pl} (in plasma)	Threshold intensity for non-thermal processes e. g. osc. 2-stream ; electron-ion decay		$E^2/8\pi$ (in plasma)	Internal kinetic energy $n_e kT_e$		
$\Phi_{pl} \simeq (10 \to 40) \times \Phi_0$	$\Phi_{thresh} \sim 10^{11} \text{ W/cm}^{-2}$		$\sim 30 \text{ J/cm}^{-3}$	$0.2 \to 1.5 \text{ kJ/cm}^{-3}$		

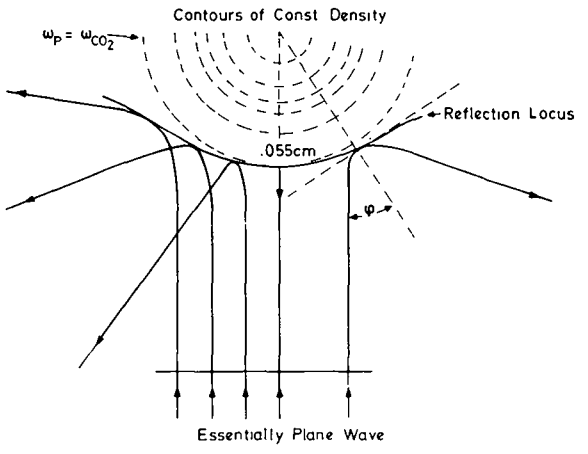

FIG. 9. — Schematic of refracted rays from CO_2 laser pump beam at the time of peak compression during the dense pinch phase of the plasma focus. CO_2 ray paths :

$$\omega^2_{co_2} = \omega^2_p(r) + c^2(k^2 + K^2_{inc} \sin^2 \varphi)$$

Reflection Points : ($K_r = 0$)

$$\omega_p(r) = \omega_{co_2} \quad \varphi.$$

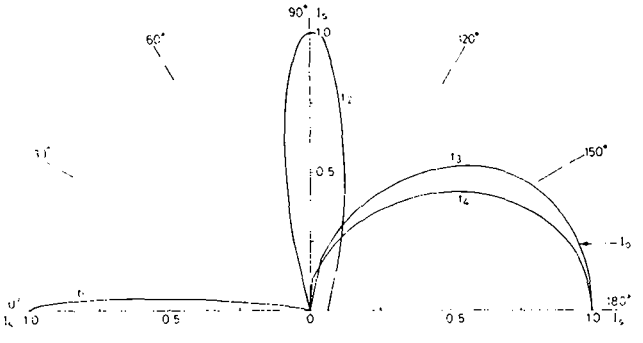

FIG. 10. — Theoretical model for the refracted light, intensity I_s, from a CO_2 laser pump beam during the dense pinch of the plasma focus. I_s is normalised to the peak of the angular intensity distribution at different times, t_1 through t_4, during the compression. The CO_2 laser operates in the TEM (0, 0) mode with a focal spot diameter, d, of 750 μm. The density distributions corresponding to $\hat{n}_e$ and r (plasma) are parabolic.

	$\hat{n}_e$	r	d
t_1 : 4.0	$\times 10^{18}$ cm^{-3}	0.5 cm	0.075 cm
t_2 : 1.03	$\times 10^{19}$ cm^{-3}	0.2 cm	0.075 cm
t_3 : 1.75	$\times 10^{19}$ cm^{-3}	0.15 cm	0.075 cm
t_4 : 3.5	$\times 10^{19}$ cm^{-3}	0.1 cm	0.075 cm

In practice, the interaction of the CO_2 beam is quite different from what has been anticipated (above) on the basis of a cylindrical plasma with a smooth density gradient and classical resistivity. The results of the irradiation experiments are as follows :

(i) Transmission of the paraxial rays is interrupted for a period of about 80 nanoseconds centred around peak compression. This cut-off in transmission, figure 11, corresponds approximately to the duration for which the plasma is over dense i. e.

$$n_e > n_{ec} = 9.94 \times 10^{18} \text{ cm}^{-3}.$$

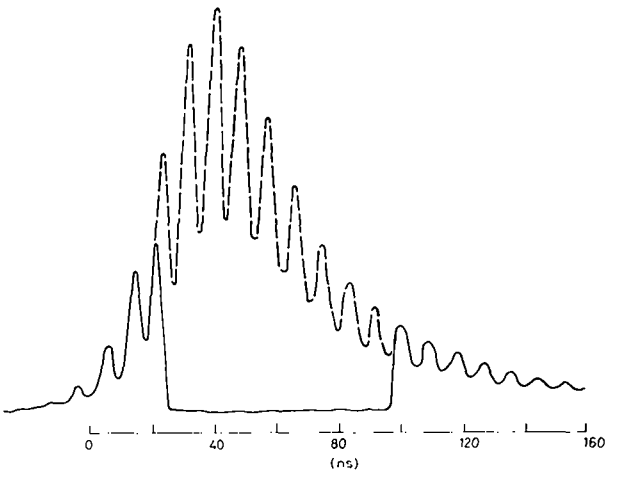

FIG. 11. — Oscillogram of transmitted CO_2 beam intensity during gainswitched pulse ; -------- corresponds to absence of absorbing medium ; ——— corresponds to transmission during dense pinch phase of the plasma focus. Note cut-off in transmission due to plasma when $n_e > n_{ec}$.

Less than one per cent of the incident light Φ_0 is backscattered.

(ii) The refracted intensity, Φ_{ref}, of the pump beam is extremely low being of the same order as the scattered intensity from the underdense outer layers of the plasma i. e.

$$\Phi_{ref} \sim \Phi_0 \, \sigma_T \, d\Omega \int_{\infty}^{r_{co}} r n_c(r) \, dr .$$

This result appears to be independent of the value of Φ_0 up to the maximum intensity used. It is also independent of the plane of polarisation of the incident pump beam ; both s$^-$ or p-type polarisation have been used. The poloidal distribution of Φ_{ref} does not change sharply in time as predicted.

(iii) No gross changes in the operation of the focus, such as the dI/dt characteristic or the neutron yield (in D_2) has been detected when the plasma is irradiated by the CO_2 beam. This is not unexpected since the high thermal conductivity of the electrons will ensure that any fractional change in the heat content due to laser energy absorption is quickly redistributed.

(iv) However, two clear indications of non-linear processes have been observed and those are correlated with absorption of the CO_2 beam by the plasma. Firstly, we observe an increase by about a factor of two in the intensity of the hard x-rays ($E > 70$ keV), presumably due to accelerated electrons striking the central anode. The second feature, which is the subject of most of the remainder of this paper, is an enhancement of the collectively scattered light from a visible (ruby) laser probe.

4. **Discussion of CO_2 Laser Beam Absorption.** — In addition to resistive absorption, direct resonance coupling between the EM wave and the electron

plasma waves can lead to enhanced absorption at oblique incidence [19]. Maximum resonance absorption can occur for small angles given by

$$\theta_{res} = \sin^{-1}\left(0.8(K_{CO_2} L)^{-1/3}\right). \quad (5)$$

Typical scale lengths in this experiment are ~ 0.2 cm so that θ_{res} is close to the experimental angle of incidence set by the F/5.5 focussing lens, figure 8. Appreciable resonance absorption can occur even in under-dense plasma where it is associated with multiple reflections between stratified layers [20]. We anticipate therefore that the refracted 10.6 μm energy, while finite, will be considerably less than the value, equation (3), calculated from resistive absorption alone.

Resonance absorption is ineffective for the paraxial rays and it is this part of the beam energy which will reach the critical density layer and give rise to non-linear heating. Enhanced absorption of the pump radiation has been predicted in the presence of the decay instability [21] and in view of the consistency of the ruby scattering observations, section 5, with this non-linear process, it may well explain the absence of backscatter in our experiments.

In solid target irradiation experiments corrugation of the critical density surface by the ponderomotive force of the pump beam has been treated theoretically [22, 23]. These authors find that enhanced resonance absorption can result if radiation is trapped in the ripples induced by the laser light pressure. High energy electrons can be generated by a number of mechanisms [24], including acceleration by the electric fields, associated with local plasma oscillations which are created by resonance absorption.

However, in the present experiments the radiation pressure is generally much lower than considered by these authors unless self focussing or *hot spots* occur in the irradiated plasma. Also we observe almost complete loss of the outer regions of the beam which should be refracted well away from the critical surface.

Non-linear, self focusing of the pump beam has been treated by Kaw *et al.*, (1973) [25]. In a slab plasma with $v_\sim/v_{th} \sim 0.02$, the plasma length required for self-focusing [26] is several cms, which is longer than our characteristic plasma dimensions. In our conditions, with nearly parabolic density distribution, filamentation of the pump beam is therefore unlikely.

The possibility of a highly-resistive and therefore absorbing region with $n_e \ll n_{ec}$ at larger radii and lower density than the compressed pinch has been raised by recent probe experiments in the plasma focus [27]. The abrupt onset of loss in beam transmission which we observe when $n_e \simeq n_{ec}$ tends to discount this explanation.

In summary we can say that the interruption of the transmitted pump beam and the observation of enhanced visible light scattering from electron waves is to be expected in these experiments. On the other hand the extremely low level for the refracted pump beam intensity lacks a convincing explanation and more experimental work, with fine-scale, angular resolution of the reflected and scattered light is required, as in the studies of Donaldson *et al.* (1976) [28].

5. **Light Scattering from Induced Langmuir waves.** — Among several instabilities which can arise at relatively low threshold irradiance as a result of strong coupling between the incident light and plasma waves perhaps the most important, apart from optical resonance [19], are the parametric, electron-ion (convective) decay instability (EID) and the oscillating two-stream (absolute) instability (OTS). Either of these mechanisms being operative, Langmuir waves will be driven in the direction of the E field polarisation vector of the pump beam. Stimulated Brillouin scattering with a slightly higher threshold is also a possibility especially since this instability can take place in the under-dense plasma region. Absence of a measurable backscatter of the incident beam due to ion-acoustic fluctuations tends to make us discount this instability in the present experiments. Figure 12 illustrates the geometry chosen to detect ruby laser

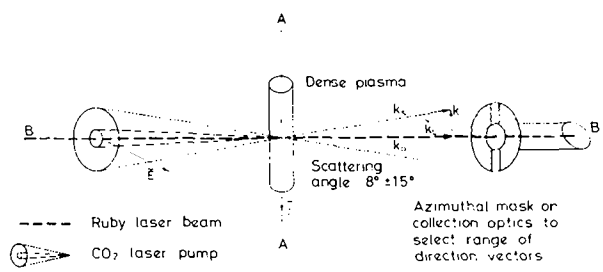

FIG. 12. — Schematic diagram of CO_2 pump beam and ruby laser probe beam relative to axis of symmetry, AA, of the focus device. Scattered ruby light is collected in the forward direction at 8° to the incident beam. The azimuthal mask can be rotated to select $\bar{K}_L$ vectors which are parallel to the polarisation vector E of the CO_2 laser.

light scattered preferentially from the induced electron waves. We discriminate against waves due to optical resonance coupling by probing only those waves $\bar{K}_L$ which are orthogonal to $\bar{\nabla} n_e$. Likewise, $\bar{K}_L$ is orthogonal to $\bar{j}$ and to current-driven ion acoustic waves.

Experimentally scattering from the electron waves will show up as a rather narrow spectral feature, shifted from the ruby frequency ω_0 by an amount given by

$$\omega_L = \omega_{CO_2} - \omega_i . \quad (6)$$

Inserting the dispersion relation for the Langmuir waves, ω_L, the ion acoustic waves, ω_i, we have

$$\omega_{pe}[1 + 3(K_L/K_D)^2]^{1/2} = \omega_{CO_2} - 1.8\left(\frac{m_e}{m_i}\right)^{1/2} \cdot \left(\frac{K_L}{K_D}\right) \cdot \omega_{pe} \quad (7)$$

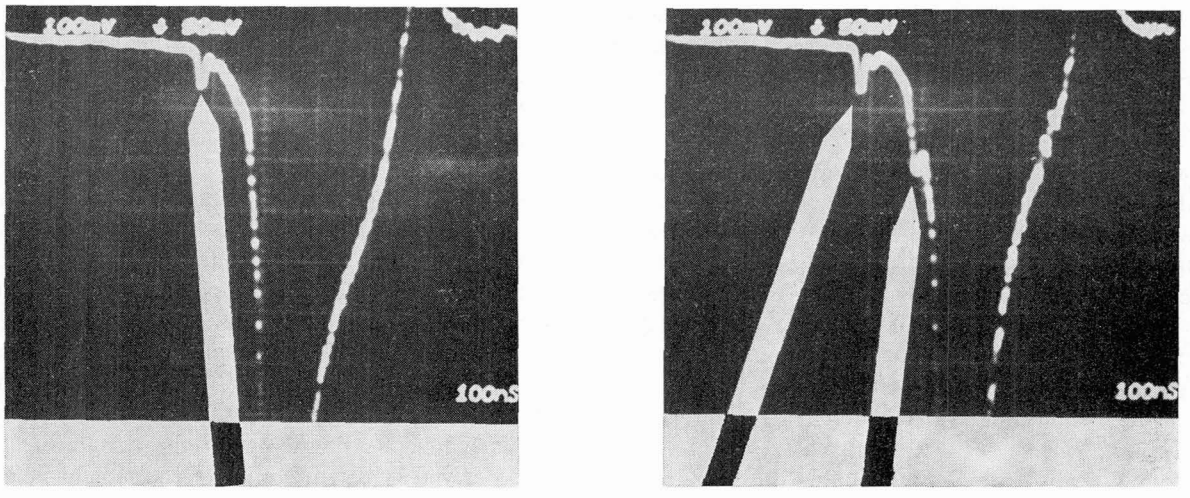

FIG. 13. — Light signal accepted by photomultiplier in the ruby laser scattering optics (Fig. 8). A photodiode provides a prompt, monitor signal of the ruby laser pulse, 35 nanoseconds before peak compression of the pinch. Scattered light signal and background light from the plasma are delayed 110 ns relative to prompt pulse. (*a*) No CO_2 laser irradiation ; (*b*) CO_2 laser focused on pinch.

where ω_{pe} is the local plasma frequency and the ratio of the inverse Debye length, $K_D = 1/\lambda_D$, to the Langmuir wave number, $K_L = 2\pi/\lambda_L$, i. e. (K_D/K_L), can be identified with the scattering parameter α. In our experiment with a mean scattering angle, $\theta = 8°$ and $\alpha \simeq 10$ then the differential scattering vector

$$|\bar{K}| = |\bar{\bar{K}}_0 - \bar{\bar{K}}_s| = \frac{K_D}{\alpha} = 1.26 \times 10^4 \text{ cm}^{-1} . \quad (8)$$

The frequency shift imposed on the scattered ruby light due to scattering from the electron waves, is from equation (7),

$$\omega_L \simeq \omega_{CO_2} = 1.78 \times 10^{14} \text{ s}^{-1} \quad (9)$$

corresponding to a wavelength shift of,

$$\Delta\lambda = \pm 427.4 \text{ Å} .$$

A narrow band filter, accepts scattered light in the region 6 500 (± 25) Å, is inserted in the scattering optics, figure 8, to suppress spuriously scattered laser light and background light from the discharge.

Under conditions of *no* pump irradiation no signal above the noise level was measured indicating that the background intensity of Langmuir waves in the unpumped plasma is not more than a factor of two or so above the thermal level.

Similar conclusions have been reported for the intensity of the ion waves by Forrest and Peacock (1974) [13]. When irradiated by the pump beam, however, the intensity of the ruby light scattered from electron waves *is* observed, figure 13, and can reach a factor of 30 above the thermal level as the pump intensity is increased beyond a threshold of about 3×10^9 W/cm^{-2}, in vacuo.

Figure 14 shows the effect of the CO_2 laser pump intensity on the intensity of the scattered probe light at a time corresponding to 30 ± 10 nanoseconds before peak compression. The density scale length at this time is $L \sim 0.2 \pm 0.05$ cm and the density, $n_e \sim 10^{19}$ cm^{-3}, is sufficiently high for frequency matching of the pump and the electrostatic plasma waves according to equation (7). No scattered signal is observed above the thermal level at times earlier

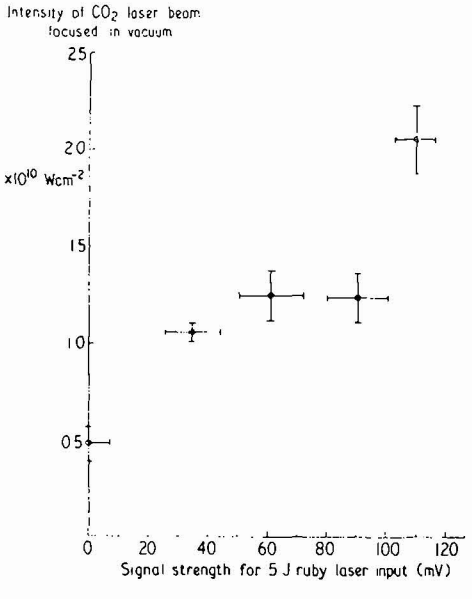

FIG. 14. — Intensity of light scattered from ruby laser by electron waves, as a function of CO_2 laser pump intensity.

in the pinch compression when $n_e \ll n_{cc}$, even with maximum pump power. Again, no enhanced scattering is observed at peak compression when, although $n_e \lesssim n_{cc}$, the density scale length, L, has decreased to 0.03 cm.

A summary of the time-dependence of the scattered light signal is shown schematically in figure 15 up to the time $t = 0$ ns when maximum compression occurs.

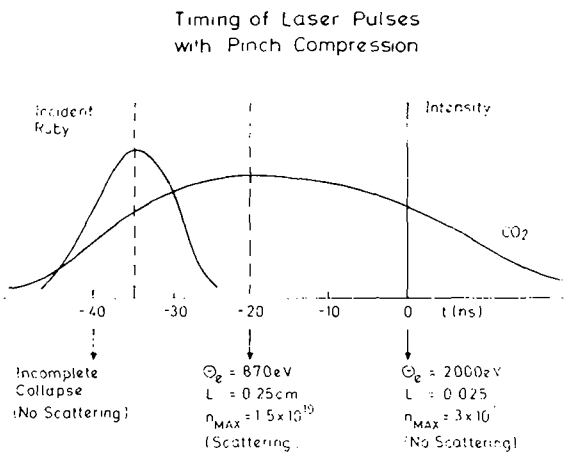

FIG. 15. — Summary of plasma parameters and relative durations of CO_2 and ruby laser pulses during the compression phase of the plasma focus.

6. **Intensity of the Induced Langmuir waves.** — Consideration of the processes giving rise to enhanced intensity in the electrostatic waves indicated that « OTS » and « EID » instabilities require about the same threshold intensity. This is set by the requirement that wave growth exceeds losses due to damping and convection out of the interaction region. In its simplest form the threshold intensity is reached when

$$(v_\sim/v_{th})^2 > \gamma/\omega_{pe}\,, \qquad (10)$$

where γ is the electron wave damping rate. Using the analysis of Perkins and Flick (1971) [29] for an inhomogeneous plasma, where $T_e \gg T_i$, the threshold for EID is

$$(v_\sim/v_{th})^2 \gtrsim (1 + 3\,T_i/T_e)\frac{8}{K_L.L}\left(\frac{\gamma_i}{\omega_i}\right)^{1/2} + \\ + 3.2\left(\frac{\gamma_i}{\omega_i}\right)\left(\frac{\nu_e}{\omega_{pe}}\right) \qquad (11)$$

ν_e is the effective electron-ion collision frequency and γ_i the ion damping frequency. In our experiment $(v_\sim/v_{th}) < 0.1$ and terms of the order $(K_L.L)^{-1}$ tend to restrict the wave growth, rather than collisional processes. The threshold pump intensity when the swelling of the pump wave, equation (4), is taken into account is Φ_{th} (vacuo) $\sim 3 \times 10^9$ W/cm^{-2} ; close to the observed value, figure 14. It is worth noting that when $L < 0.05$ cm which occurs close to peak compression, figure 4, then Φ_{th} (vacuo) exceeds the available pump power. More recently, Goldman and Rudolph in [30], have calculated the linear growth of electron waves driven by the EID instability and their convection in an inhomogeneous $T_e = T_i$ plasma, using WKB theory and including swelling of the pump intensity. Their derivation of the threshold intensity agrees with equation (11) and their derivation of the *absolute* intensity allows a direct comparison with the observed scattering cross-sections. Firstly, however, we require to calculate the plasma volume responsible for the scattered light signal. Each radial layer, within which the frequency match, equation (6), is satisfied, will contribute to the intensity of the electron feature.

The total spread in frequency of the electron feature is made up of a shift from the pump frequency equal to $\pm\,\omega_i$, the ion acoustic frequency, and a broadening $\delta\omega_m$ due to an allowed mismatch

$$\delta\omega_m = PK_L\,v_e(m_e/m_i)^{1/2}/\sqrt{2} \qquad (12)$$

where P is the pump intensity above threshold. There is in addition, a spread in frequency due to the finite range of wave vectors accepted by the scattering optics. Typically, the ion acoustic frequency, ω_i, produces a wavelength shift of 0.5 → 1.0 angstrom and the total broadening $(\delta\omega_m + \delta\omega_{optics})$ amounts to a few angstroms. The incremental plasma radius contributing to the electron feature is therefore

$$(\omega_i + \delta\omega_m + \delta_{optics})\left|\frac{\partial\omega_{pe}}{\partial r}\right|^{-1}. \qquad (13)$$

This radial increment is defined in figure 16 by the inner boundary r_{co} at which $\omega_L = \omega_{CO_2}$ and an outer boundary r_f, where the frequency match condition, equation (6), can just be satisfied. A typical value for $r_{co} - r_f$ is 100 microns which is considerably smaller than the radial increment viewed by the 50 Å band-pass filter. An enhancement of 30 above the thermal level is observed, averaged over the 50 Å volume ; it would appear therefore that much higher wave intensities is to be expected locally, within $r_f - r_{co}$.

A plot of the radial variation of the plasma frequency and of the scattering parameter $\alpha = K_D/K$, emphasises the constraints in real space and time over which the conditions for enhanced scattering from either EID or OTS driven electron waves can be satisfied. As shown in figure 17 the density is only sufficiently high for a frequency match between the pump EM beam and electron plasma oscillations within the 40 nsecs prior to peak compression.

Typically within this period $\omega_{pe} = \omega_{CO_2}$ at a plasma radius $r_{co} \sim 0.02$ cm where the scattering parameter $\alpha \simeq 15$. This high value of α ensures that Landau damping of the electron waves is negligible compared to resistive damping. (The ion waves are heavily Landau damped since $T_e \simeq T_i$.) On the other hand

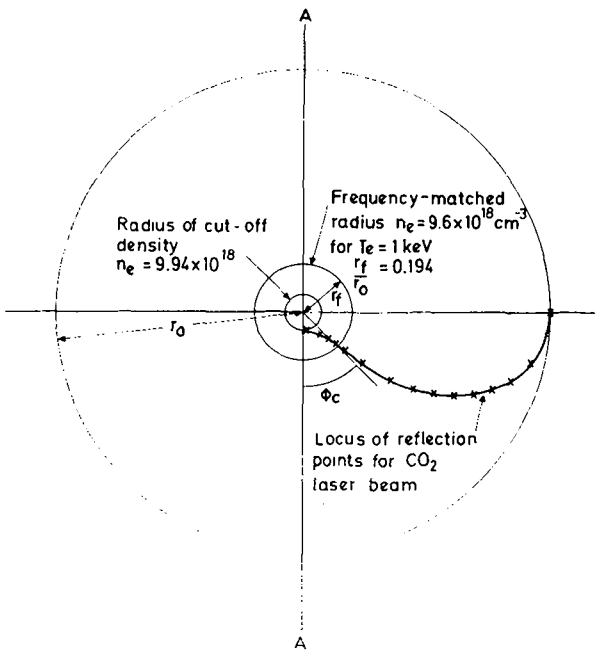

FIG. 16. — Locus of reflection points calculated for CO_2 laser beam parallel to AA and parabolic density profile with peak density 1×10^{19} cm^{-3}. Paraxial rays along AA penetrate deepest towards the cut off radius r_{co}, where

$$n_{ec} = 9.94 \times 10^{18} \text{ cm}^{-3} .$$

The frequency matched radius r_f, for the electron ion decay instability is also shown. The locus of reflection points makes an angle $\varphi_c \sim 45°$ to AA.

the intensity in the electron feature is $\propto 1/\alpha^2$ and the scattered signal level could be improved by increasing the scattering angle, while keeping the restriction of $\alpha \lesssim 5$. The inner hatched area, figure 17, represents the small area at peak compression where the WKB approximation breaks down. In order that a WKB description be valid, then

$$\lambda_L \frac{\partial \lambda_L}{\partial r} \ll \lambda_L . \tag{14}$$

From the Bohm Gross dispersion relation for electron waves,

$$\omega_L = [\omega_{pe}^2(1 + 3/\alpha^2)]^{1/2} \tag{15}$$

i. e.

$$\frac{\partial \lambda_L}{\partial r} = \frac{\pi \alpha^2}{3 K_L . L} \quad \text{i. e.} \quad \alpha^2 \ll K_L L . \tag{16}$$

This relation, equation (16), is satisfied for $n_e \lesssim n_{cc}$ during the 40 nsecs up to peak compression, figure 17.

The scattering volume, which will lie within the radial increment $(r_f - r_{co})$, can be defined as $v_s = lA_s$, l is the axial length equal to the CO_2 focal shot size and

$$A_s = 2 . \delta\theta_s . r . \delta r \tag{17}$$

where $\delta\theta_s$ is the range of accepted scattering angles i. e. 5°, and r is determined by the time at which

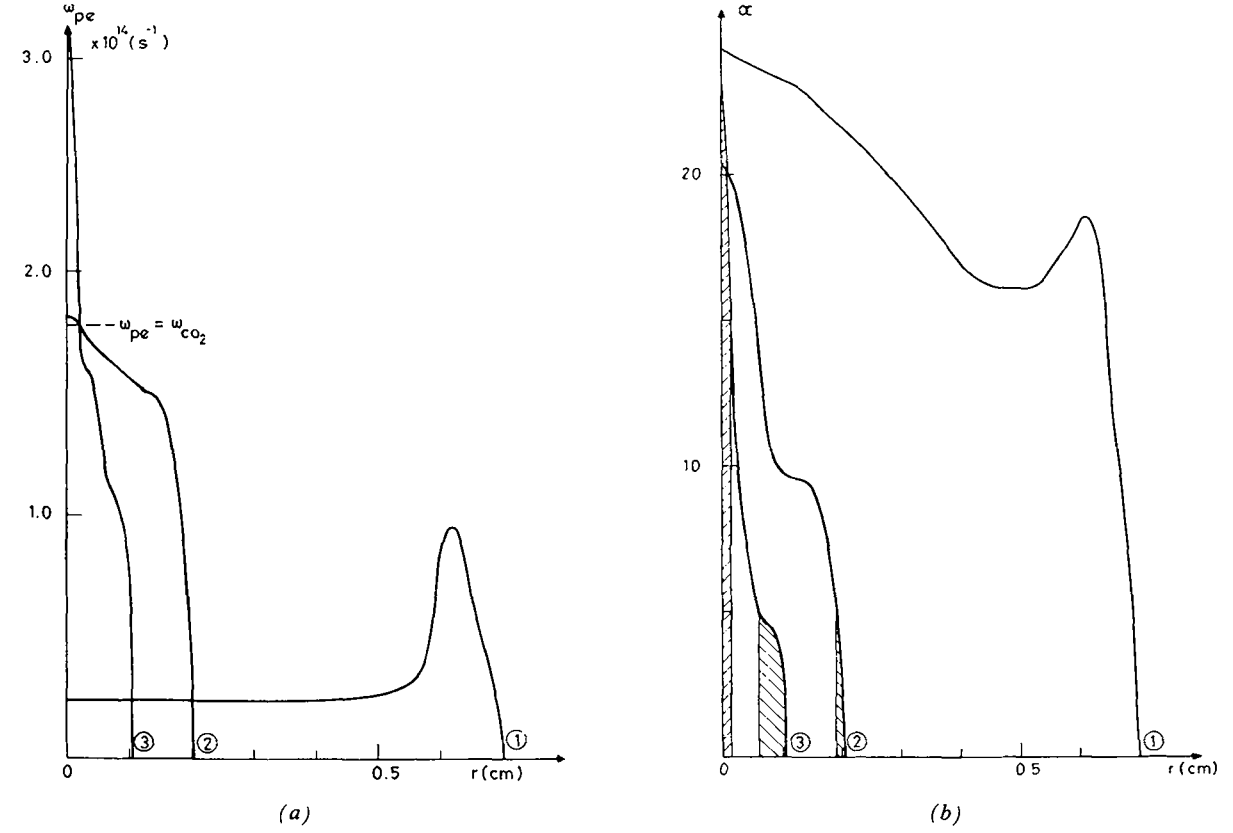

FIG. 17. — Spatial variation of the scattering parameter α and of ω_{pe} during the pinch phase. ω_{pe} is calculated from sample interferograms of the density profile (1) $t = -60$ ns ; (2) $t = -35$ ns, (3) $t = 0$. //// WKB theory inapplicable, at $t = 0$. \\\\ electron waves Landau damped.

the Langmuir intensity is $\frac{1}{2}$ of its value, $I(t_f)$ at its turning point.

In figure 18*b* we illustrate the curved scattering volume by an equivalent slab with the orthogonal Langmuir wave number $K_y = K_L = K_D/\alpha$. In this figure x_0 is the reflection point.

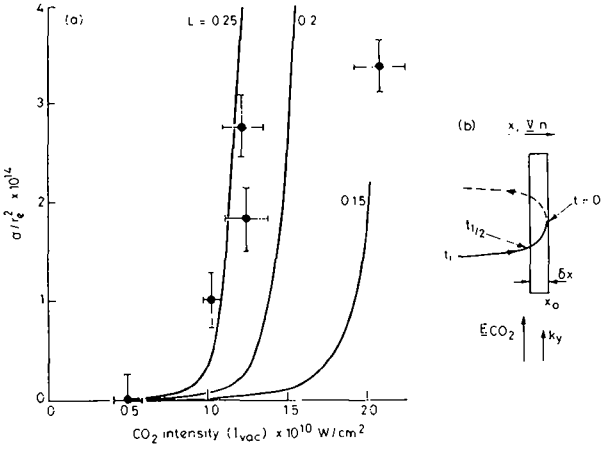

FIG. 18. — (*a*) Plasma scattering cross section as a function of focussed CO_2 laser intensity. Experimental points are compared with predictions of WKB theory with the parameter density scale length, L, assuming values of 0.25, 0.2 and 0.15 cm and with a constant value of $T_e = 300$ eV. (*b*) Langmuir ray paths.

Integration along the ray path from an initial time t_i, at which the net growth rate is zero and $I(t_1)$ is unity, to a final time t_f at which the Langmuir wave is reflected, gives

$$I(t_f) = \left[\frac{\alpha(m_i/m_e)^{1/2}}{1.7}\right] \exp\left[\frac{5}{256} \cdot LK_y \cdot \frac{\bar{E}^2}{nKT_e}\right] . \quad (18)$$

The exponent contains the local CO_2 laser electric field strength, $\bar{E}^2$, modified from the vacuum intensity by absorption and by the geometric optics swelling factor. The dominant term in the wave amplitude is the spontaneous beat emission which leads to fluctuation levels which are several orders of magnitude above thermal and which are confined to a very limited region in space with $\delta r \simeq 5 \times 10^{-4}$ cm i. e. $\ll r_f - r_{co}$.

The integrated scattering cross section is given approximately by

$$\sigma = (r_e/\alpha)^2 . n_e . V_s . \delta\Omega_s . I(K) . \quad (19)$$

Here r_e is the electron radius and $\delta\Omega_s$ is the solid angle subtended by the scattering optics.

$$I(K) = \lim_{V \to 0} < | \delta E(K) |^2 > /4 \pi nkT.V$$

is the spectral intensity of the longitudinal field fluctuations normalised to unity in equilibrium.

Evaluation of all the quantities in equation (19) leads to the plots for σ/r_e^2 shown in figure 18*a* with the scale length L as a parameter. T_e is assumed to be 300 eV and the frequency matched density 9.8×10^{18} cm^{-3}. The observed scale length $L = 0.25$ cm gives about the best fit with the theory at least up to the intensity where one might expect the linear saturation theory to break down.

In summary, the calculated threshold for the parametric electron ion — decay instability and its dependence on scale length is consistent with the experiment ; and the inhomogeneous linear saturation theory appears to give a fairly satisfactory fit to the data at CO_2 laser intensities around 10^{10} W/cm^{-2} and below. A definite identification of the electron-ion decay instability may be resolved with further measurements, particularly of the *off set* frequency difference between the Langmuir waves and the driving CO_2 laser frequency.

Finally, it is interesting to note that broadly similar experimental results have been reported in quite independent plasma focus experiments [31] by Tanimoto and co-authors (1976), using somewhat higher CO_2 laser irradiation intensities. These authors conclude that the parametric instability is the most likely cause of induced Langmuir waves.

References

[1] PEACOCK, N. J. *et al.*, 3rd IAEA Conf. on *Plasma Physics and Controlled Nuclear Fusion Research*, Novosibirsk, Proceedings **2**, 51-65 (Published IAEA Vienna) (1969).

[2] SIGEL, R., EIDMANN, K., PANT, H. C., SACHSENMAIER, P., *Phys. Rev. Lett.* **36** (1976) 1369.

[3] YAMANAKA, C., Proceedings of Seminar on Laser Interaction with Matter, 32-50. Institute of Laser Engineering, Osaka University (1977).

[4] OFFENBERGER, A. A., CERVENAN, M. R., YAM, A. M., PASTERNAK, A. W., *J. Appl. Phys.* **47** (1976) 1451-1458.

[5] DUBOIS, D. F. and GOLDMAN, M. V., *Phys. Rev. Lett.* **14** (1965) 544-546.

[6] DUBOIS, D. F. and GOLDMAN, M. V., *Phys. Rev.* **164** (1967) 207-222.

[7] GOLDMAN, M. V., *Ann. Phys.* **38** (1966) 117-169.

[8] NISHIKAWA, K., *J. Phys. Soc. Japan* **24** (1968) 1152-1158.

[9] MORGAN, P. D. and PEACOCK, N. J., Proceedings of 2nd Topical Conference on Pulsed High Beta Plasmas, Garching (1972) 179-182 (Max Planck Inst. für Plasmaphysik, IPP 1/127).

MORGAN, P. D., « Optical Refractivity Studies of Plasma Focus », Ph. D Thesis, University of London (1974).

[10] PEACOCK, N. J., HOBBY, M. G. and MORGAN, P. D., Proceedings of 4th Int. Conf. on *Plasma Physics and Controlled Nuclear Fusion Research* (Published IAEA Vienna) Vol. 1, 1971 537-552.

[11] BERNARD, A. *et al.*, 5th IAEA Conf. on *Plasma Physics and Controlled Nuclear Fusion Research*, Tokyo, Proceedings (Published IAEA Vienna) **3** (1975) 83-98.

[12] BERNARD, A. *et al.*, *Phys. Fluids* **18** (1975) 180-194.

[13] FORREST, M. J. and PEACOCK, N. J., *Plasma Phys.* **16** (1974) 489-498.
[14] EVANS, D. E., *Plasma Phys.* **12** (1970) 573.
[15] POTTER, D. E., *Phys. Fluids* **14** (1971) 1911-1924.
[16] KURIKI, K. and PEACOCK, N. J., « Plane-polarised CO_2 laser beam from an unstable confocal resonator », Culham Report CLM-P446 (1976).
[17] SHEARER, J. W., *Phys. Fluids* **14** (1971) 183-185.
[18] DAWSON, J., KAW, P. and GREEN, B., *Phys. Fluids* **12** (1969) 875-882.
[19] FREIDBERG, J. P., MITCHELL, R. W., MORSE, R. L. and RUDSINSKI, L. I., *Phys. Rev. Lett.* **28** (1972) 795-799.
[20] MUELLER, M. M., *Phys. Rev. Lett.* **30** (1973) 582-585.
[21] DUBOIS, D. F., GOLDMAN, M. V. and MCKINNIS, D., *Phys. Fluids* **16** (1973) 2257-2269.
[22] FORSLUND, D. W., KINDEL, J. M., LEE, K., LINDMAN, E. L., *Phys. Rev. Lett.* **36** (1976) 35-38.
[23] KINDEL, J. M., LEE, K., LINDMAN, E. L., *Phys. Rev. Lett.* **34** (1975) 134.
[24] BEZZERIDES, B., DUBOIS, D. F., FORSLUND, D. W., KINDEL, J. M., LEE, K. and LINDMAN, E. L., 6th IAEA Conf. on Plasma Physics and Controlled Nuclear Fusion Research, Berchtesgaden. Proceedings series. Supplement Vol. 1, 123-129 (Published IAEA Vienna) 1977.
[25] KAW, P., SCHMIDT, G. and WILCOX, T., *Phys. Fluids* **16** (1973) 1522-1525.
[26] HAAS, R. A., BOYLE, M. J., MANES, K. R., SWAIN, J. E., *J. Appl. Phys.* **47** (1976) 1318-1321.
[27] BERNARD, A. *et al.*, 6th IAEA Conf. on *Plasma Physics and Controlled Nuclear Fusion Research*, Berchtesgaden. Proceedings series. Supplement Vol. 3, 471-482 (Published IAEA Vienna) 1977.
[28] DONALDSON, T. P., HUBBARD, M., SPALDING, I. J., *Phys. Rev. Lett.* **37** (1976) 1348-1351.
[29] PERKINS, F. W. and FLICK, J., *Phys. Fluids* **14** (1971) 2012-2018.
[30] FORREST, M. J. *et al.*, *Phys. Rev. Lett.* **37** (1976) 1681-1684.
[31] TANIMOTO, M., KOYAMA, K., MATSUMOTO, Y. and SUGIURA, M., 6th IAEA Conf. on *Plasma Physics and Controlled Nuclear Fusion Research*, Berchtesgaden. Proceedings series. Supplement Vol. 2 605-612 (Published IAEA Vienna) (1977).